Available online at www.sciencedirect.com
SCIENCE DIRECT®
Acta Materialia 53 (2005) 1191–1204
Acta MATERIALIA
www.actamat-journals.com

Simulation of faceted film growth in three dimensions: microstructure, morphology and texture

Peter Smereka [a,*], Xingquan Li [b], Giovanni Russo [c], D.J. Srolovitz [d]

[a] Department of Mathematics, University of Michigan, 525 East University Ave, Ann Arbor, MI 48109-1109, USA
[b] Department of Physics, University of Michigan, Ann Arbor, MI 48109, USA
[c] Department of Mathematics, University of Catania, Italy
[d] Department of Mechanical and Aerospace Engineering, Princeton University, Princeton, NJ 08544, USA

Received 28 September 2004; received in revised form 3 November 2004; accepted 6 November 2004
Available online 22 December 2004

Abstract

We present the results of a series of simulations of the growth of polycrystalline, faceted films in three spatial dimensions. The simulations are based upon the assumptions of the well known van der Drift model in which the growth rate of each surface is fixed only by its crystallographic orientation. The simulation method is based upon the level-set formalism and the only input are the relative velocities of the different facets. We focus specifically on cubic crystals that expose only {1 1 1} and {0 0 1} facets, such as diamond. Results are presented for the temporal evolution of the surface morphology, microstructure, mean grain size, grain size distribution, and crystallographic texture. The mean grain size and surface roughness increase with film thickness h as $h^{2/5}$, in agreement with theoretical results. The grain size distribution is self-similar. The films all exhibit a columnar microstructure and a fiber texture that sharpens as the film grows. The orientation of the texture is determined by the facet growth velocity ratio. The new simulation method is equally applicable to any type of faceted film growth.

Keywords: Thin-film growth; Level-set method; Microstructure; Morphology

1. Introduction

The growth of polycrystalline films is central to a wide range of modern technologies. In fact, outside of the microelectronics industry, most technologically important films and coatings are polycrystalline rather than single crystals or amorphous (polycrystalline films are also widely used in microelectronics). A wide range of techniques has been employed to grow polycrystalline films, including electron beam deposition, molecular beam epitaxy, chemical vapor deposition, magnetron sputtering, etc. In many cases, the resultant films are strongly faceted, generally exhibiting faces corresponding to low index crystallographic planes. The growth rate of the different facets may depend on several factors, including their inclination relative to the deposition flux, sticking coefficients, site specific reaction rates, etc. In this paper, we examine the situation in which the growth rate (velocity) of each facet depends only on the crystallographic orientation of the facet. This is interface-limited growth and is common in, for example, the chemical vapor deposition (CVD) of diamond. This idealization of the growth process was suggested by van der Drift [1] (it is often referred to as the van der Drift model) and even earlier by Kolmogorov [8]. In this paper, we perform a series of simulations of the growth of polycrystalline, faceted films and examine the implications of this model for the evolution of the

* Corresponding author. Tel.: +1 734 763 5724; fax: +1 734 763 0937.
E-mail address: psmereka@umich.edu (P. Smereka).

1359-6454/$30.00
doi:10.1016/j.actamat.2004.11.013

microstructure and morphology of such films in three spatial dimensions using a level-set technique.

In many film growth scenarios, such as diamond CVD, the film develops a fiber texture (i.e., a particular crystallographic direction is normal to the substrate, but the crystal orientation of the film grains parallel to the substrate is random). For example, if each grain has its $\langle 1\,1\,1\rangle$ direction oriented normal to the substrate, such a crystal has a $\langle 1\,1\,1\rangle$ fiber texture. The development of a fiber texture during polycrystalline film growth is a natural consequence of the van der Drift [1], faceted growth model. In this model, each crystallite or grain grows with each crystallographically equivalent facet moving with a known normal velocity until a facet meets the surface of another growing crystallite. When surfaces of different grains meet, a grain boundary is formed. We will assume that the resultant grain boundaries are immobile. A fiber texture develops because the edges of faceted crystallites grow faster than faces and corners grow faster than edges. If we consider a substrate on which are placed infinitesimally small crystallites with random orientations, the ones with the corners pointing normal to the substrate will have the largest growth velocity perpendicular to the substrate. Since these crystallites or grains grow fastest, they will outgrow their neighboring grains and, hence, win the growth competition. As time proceeds the growth front is increasingly composed of grains with these fastest growing orientations – this is the fiber texture. This process is sometimes referred to as geometric selection. Thompson [2] discusses these issues in his review article on polycrystalline films.

Wild et al. [3,4], Dammers and Radelaar [6], Paritosh et al. [7] developed algorithms for simulating the growth of faceted crystals based on the van der Drift model in two dimensions. Dammers and Radelaar demonstrated that the average grain size, d, grows as $d \sim \sqrt{h}$, where h is the film thickness. Paritosh et al. [7] did a more detailed study and showed, among other things, that the earlier results were valid for different types of faceted crystals. They also found that the grain size distribution was invariant upon scaling the grain size with the film height. We also note that Kolmogorov [8] and Thijssen et al. [9] predicted that in two dimensions $d \sim \sqrt{h}$ as $h \to \infty$ on theoretical grounds. In three dimensions, Thijssen [10] predicted $d \sim h^{2/5}$. In addition, Thijssen [10] performed computations on a simplified version of the van der Drift model and showed that they were in agreement with his analytical prediction. In these computations, Thijssen considered the crystallites as cones or cubes. The growth front of the polycrystalline film was first approximated as the outer envelope of all such cones or cubes. The difficulty with this approximation is that one crystal can interpenetrate through another crystal and then unphysically re-emerge. Thijssen overcame this difficulty by tagging crystal tops that have disappeared. Tagged tops are not allowed to re-emerge, but other parts of the crystal have the possibility to re-emerge. The computations were in agreement with the prediction that $d \sim h^{2/5}$. Barrat et al. [11] used crystal shapes as shown in Fig. 1 and approximated the growing film as the outer envelope of the individual crystals. One drawback of both these approaches is that information about the grain boundaries is lost.

In this paper, we extend the earlier simulations of faceted, polycrystalline growth from two to three space dimensions while retaining a general description of faceting and grain shape and avoiding the interpenetration problems inherent in early three-dimensional approaches. The earlier two-dimensional simulations were performed using a method that tracks the evolution of the surfaces during film growth. Such an approach is much more difficult to apply in three dimensions because of the increased topological complexity. To our knowledge, no such three-dimensional algorithm has ever been developed that fully implements the van der Drift model. In the present paper, we extend the level set method for faceted polycrystal growth originally developed by Russo and Smereka [12] that altogether avoids issues of topological complexity. We then apply this model to the case of chemical vapor deposition of polycrystalline diamond films. Specifically, we examine the evolution of the surface morphology, polycrystalline grain structure, grain size distribution and crystallographic texture.

2. Diamond

In the paper, we shall focus on the case of a cubic material that exhibits only $\{0\,0\,1\}$ and $\{1\,1\,1\}$ facets, as

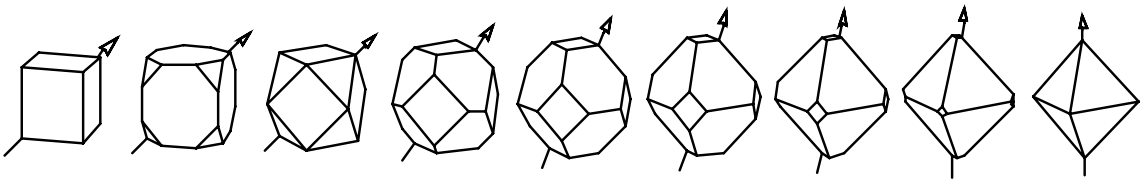

Fig. 1. The idiomorphs or, equivalently, the kinetic Wulff shapes for diamond as a function of the facet growth velocity ratio, α. Moving from left to right, α increases from 1 to 3, in step of 0.25. All idiomorphs are identical for $\alpha \leqslant 1$; i.e., a cube with $\{0\,0\,1\}$ facets. Similarly, the idiomorphs are identical for all $\alpha \geqslant 3$: i.e., an octahedron with $\{1\,1\,1\}$ facets. The third figure from the left corresponds to $\alpha = 1.5$. The arrow indicate the fastest growing direction.

appropriate for diamond [3,4,6,7,11]. In cubic crystals, all {0 0 1} surfaces are identical and all {1 1 1} are identical. Wild et al. [3,4] showed that an isolated crystallite growing with a fixed ratio of the {0 0 1} to {1 1 1} facet normal velocity will evolve into a series of invariant shapes that are known as idiomorphs. This ratio is traditionally written as

$$\alpha = \sqrt{3}\frac{V_{001}}{V_{111}}. \tag{1}$$

The procedure for determining this shape is identical to that used to determine the equilibrium shape of a crystal via the Wulff construction, except that the surface free energy vectors are replaced with the orientation dependent growth velocity. Hence, idiomorphs are also referred to as kinetic Wulff shapes. The presence of facets in the present model implies the existence of cusps in the growth velocity versus surface orientation plot. The variation of the shape of these idiomorphs with α is shown in Fig. 1. For $\alpha \leqslant 1$, the idiomorphs are all cubes composed of {0 0 1} facets. For $\alpha \geqslant 3$, the idiomorphs are octahedra delimited by {1 1 1} facets. For $1 < \alpha < 3$, the idiomorphs are cubo-octahedron, exposing both {0 0 1} and {1 1 1} facets. For $1 < \alpha < 1.5$, the idiomorphs exhibit six octagonal {0 0 1} facets and eight triangular {1 1 1} facets. For $1.5 < \alpha < 3$, the idiomorphs exhibit six square {0 0 1} facets and eight hexagonal {1 1 1} facets. For the special case of $\alpha = 1.5$ only square {0 0 1} and triangular {1 1 1} facets are present. These geometric constructions are useful in interpreting the polycrystalline microstructures. Further, our computations will show that an interesting morphological bifurcation occurs in the polycrystalline films at $\alpha = 1.5$.

The microstructure of a polycrystalline film is determined by the growth competition between adjacent grains and the film morphology is dictated by the orientations and relative positions of the surviving grains (with orientation playing a much more important role). One expects that crystallites whose orientation is such that the fastest growing direction is perpendicular to the substrate will outgrow the crystallites with other orientations, as discussed above. The variation of the fastest growing direction with α is indicated by the arrows in Fig. 1. It is convenient to express this direction relative to the $\langle 0\,0\,1\rangle$ direction using the two polar angles, θ and ϕ from spherical coordinates. Paritosh, et al. [7] present the following expression for the fastest growing direction:

$$\theta_{\max} = \begin{cases} \tan^{-1}\sqrt{2} \approx 54.73^{\circ}, & \alpha \leqslant 1, \\ \tan^{-1}\left(\frac{\sqrt{5\alpha^2-12\alpha+9}}{\alpha}\right), & 1 \leqslant \alpha \leqslant \frac{3}{2}, \\ \tan^{-1}\left(\frac{3-\alpha}{\alpha}\right), & \frac{3}{2} \leqslant \alpha \leqslant 3, \\ 0, & \alpha \geqslant 3 \end{cases} \tag{2}$$

and

$$\phi_{\max} = \begin{cases} \frac{\pi}{4}, & \alpha \leqslant 1, \\ \tan^{-1}\left(\frac{3-2\alpha}{\alpha}\right), & 1 \leqslant \alpha \leqslant \frac{3}{2}, \\ 0, & \alpha \geqslant \frac{3}{2}. \end{cases} \tag{3}$$

One can use these expressions to show that the fastest growing direction is of the type:

$$\langle h\,k\,l\rangle_{\text{fastest}} = \begin{cases} \langle 1\,1\,1\rangle, & \alpha \leqslant 1, \\ \langle h\,1\,1\rangle, & 1 \leqslant \alpha \leqslant \frac{3}{2}, \\ \langle 0\,k\,1\rangle, & \frac{3}{2} \leqslant \alpha \leqslant 3, \\ \langle 0\,0\,1\rangle, & \alpha \geqslant 3, \end{cases} \tag{4}$$

where

$$h = \frac{3-2\alpha}{\alpha}, \quad k = \frac{3-\alpha}{\alpha}, \quad \text{and} \quad l = 1.$$

For example, if $\alpha = \frac{3}{2}$, the fiber texture is $\langle 0\,1\,1\rangle$. Eq. (4) was presented in [5,24,25].

Eq. (4), combined with Fig. 1, can be used to make several important predictions regarding the microstructure in the long time limit within the van der Drift model framework. For example, the film will develop a fiber texture where the fiber axis is given by (4).

When $\alpha \leqslant 1$, the idiomorph is a cube delimited by {0 0 1} facets. The longest vectors from the center of the idiomorph to any point on its surface are in the $\langle 1\,1\,1\rangle$ directions. Hence, we expect the microstructure to have a $\langle 1\,1\,1\rangle$ fiber texture and expose {0 0 1} facets on its surface. As α is slightly increased, the fiber texture will remain close to $\langle 1\,1\,1\rangle$, but the surface microstructure will change dramatically. It will predominantly show facets with normals nearly perpendicular to this direction, namely the triangular {1 1 1} facets (note the small triangular {1 1 1} facets in the second idiomorph from the left in Fig. 1). As α increases to 1.5, the fiber texture will change from $\langle 1\,1\,1\rangle$ to $\langle 0\,1\,1\rangle$ and the surface microstructure will evolve into a mixture of {1 1 1} and {0 0 1} facets (see the third idiomorph from the left in Fig. 1). As α is further increased to just less than 3, the surface microstructure will become dominated by square {0 0 1} facets and the fiber texture will change from $\langle 0\,1\,1\rangle$ to close to $\langle 0\,0\,1\rangle$. For $\alpha \geqslant 3$, the fiber texture will remain $\langle 0\,0\,1\rangle$, but the surface will be composed only of {1 1 1} facets.

In the next section, we present the level set method that we use to evolve three-dimensional, faceted, polycrystalline films to determine microstructure and morphology. The simulations not only verify the above discussion, but also provide images of the microstructure and morphology that can be directly compared with experimental plan view and cross-sectional micrographs as well as detailed information on texture and grain size evolution.

3. Simulation method

We now outline the derivation of our simulation method; first, for a single crystal. The method is based on two main ideas: the level set method and the Wulff construction.

3.1. Level set method

We first discuss the level set method, originally developed by Osher and Sethian [13]. In this method, the interface of crystal, Γ, is the surface on which the smooth scalar field, u, is zero:

$$\Gamma = \{u(\boldsymbol{x},t) = 0\}.$$

We shall assume that the crystal exists where the field $u < 0$ and there is a vacuum or vapor in the region $u > 0$, exterior to the crystal. If the velocity of the surface in the direction of its normal, v_n, is known, then the time evolution of u is given by

$$\frac{\partial u}{\partial t} + v_n|\nabla u| = 0.$$

For an introduction to this method the reader is referred to the books by Sethian [14] and Osher and Fedkiw [15] and the review article by Smereka and Sethian [16]. The unit normal to the interface is given by

$$\boldsymbol{n} = \frac{\nabla u}{|\nabla u|}.$$

Therefore, if the normal velocity is a function of direction, $v_n = \gamma(\boldsymbol{n})$, the time evolution of u is given by the level set equation

$$\frac{\partial u}{\partial t} + \gamma\left(\frac{\nabla u}{|\nabla u|}\right)|\nabla u| = 0. \tag{5}$$

In our model we are assuming that the normal velocity v_n is only a function of the normal $\boldsymbol{n}$ to the surface. This assumption may be a good approximation in many cases. There are some circumstances in which such approximation is not a good one. For example, if the crystals form a closed region containing vapor, then it is clear that the crystal cannot grow, since chemical vapor deposition is inhibited on the surface of such region. Here we neglect such effect.

We note in Eq. (5) the interface velocity, $v_n = \gamma(\boldsymbol{n})$, has been extended into three dimensions. Therefore, Eq. (5) can be solved on a fixed grid and the surface of the crystal is found using iso-surface rendering graphics software.

It is clear that if we wish to evolve a crystal in three space dimensions, we must solve the level set equation in three dimensions, even though its surface is two-dimensional. This can be rather expensive in terms of computer time and memory since we must update u at every location whether it is needed or not. We defer the discussion about how to efficiently use this method to later in the paper. The major remaining issue is how to implement the level set method to describe and evolve faceted crystals.

3.2. Kinetic Wulff shape

If we know the surface velocity for all possible surface normals, the location of the interface can be determined from

$$\dot{\boldsymbol{x}} = \gamma(\boldsymbol{n})\boldsymbol{n}. \tag{6}$$

This equation has a long history and the reader is referred to the articles by Taylor et al. [17], Osher and Merriman [18], Peng et al. [19] and the references therein. The important discovery made by Wulff [20] and Frank [21] is that if the crystallite shape evolves as described by Eq. (6), the shape will evolve asymptotically into the Wulff shape. The Wulff shape is the Legendre transform of γ or equivalently the inner convex hull of γ, as proved by Soravia [14] and Osher and Merriman [18]. More precisely, Osher and Merriman proved that the unique viscosity solution of Eq. (5) asymptotically approaches the Wulff shape of $\gamma(\boldsymbol{n})$. From a practical point of view this means that if one solves Eq. (5) with an upwind method (see, for example [13–16]), the zero level or contour will approach the Wulff shape. In particular, if we start with a Wulff shape and evolve it using Eq. (5), its shape will not change as it grows.

In order to use Eq. (5) for our purposes, we must find a γ function so that the Wulff shapes are those as given in Fig. 1. This is a type of inverse problem, which was solved by Russo and Smereka [12]. Suppose we have a crystal and know the normal direction and velocities of each of its facets, $\boldsymbol{n}_i$ and w_i, respectively. Then we wish to find a $\gamma(\boldsymbol{n})$ so that when it evolves as described by Eq. (5), the level set of u will be composed of facets whose normal directions and velocities are those prescribed above. This is done as follows: first we define

$$k(\boldsymbol{n}) = \arg\max_j \boldsymbol{n}\cdot\boldsymbol{n}_j,$$

then

$$\gamma(\boldsymbol{n}) = w_{k(\boldsymbol{n})} + \sigma\sqrt{1 - (\boldsymbol{n}\cdot\boldsymbol{n}_{k(\boldsymbol{n})})^2}, \tag{7}$$

where $\sigma \geqslant \sigma_0$, and σ_0 is a geometric parameter that depend on the Wulff shape. In our computations we choose $\sigma = 1.1$.

For initial conditions, we choose a u whose zero level set is a polyhedron with normal directions as prescribed above. We observe that when the system evolves as per Eq. (5), the zero level set quickly evolves to the corresponding Wulff shape. This is consistent with the predictions of Osher and Merriman [18].

3.2.1. Multiple grains

Since we are interested in modeling a polycrystalline film, we must implement the method for many separate grains. Therefore, we introduce a level set function, u_j, to describe the evolution of each grain j. We remind the reader that $u_j < 0$ inside the grain and $u_j > 0$ outside of that grain. This means that if both $u_i < 0$ and $u_j < 0$ at the same physical location and $i \neq j$ then the grains would overlap. This is clearly unphysical. Thus, we introduce the overlap function

$$\eta(\boldsymbol{x},t) = \begin{cases} 0, & \text{if any of the } u_j\text{'s overlap} \\ 1, & \text{otherwise .} \end{cases}$$

The time evolution of the level set functions is then

$$\frac{\partial u_j}{\partial t} + \eta(\boldsymbol{x},t)\gamma_j\left(\frac{\nabla u_j}{|\nabla u_j|}\right)|\nabla u_j| = 0. \tag{8}$$

We note that each grain has its own γ_j function since each grain has it own set of normals. We remark that the interface of the entire polycrystalline film can easily be computed from the individual level set functions as follows:

$$u(\boldsymbol{x},t) = \min_j u_j(\boldsymbol{x},t). \tag{9}$$

Finally we mention that if we evolve the system as per Eq. (8) with $\eta = 1$ and use Eq. (9), the zero level set of u will give the outer envelope of the individual grains growing without restriction. The interaction of the crystals is determined by the overlap function.

3.3. Computational issues

In our approach, each grain has its own level set function. For problems with a large number of grains this becomes very expensive both in terms of computer time and memory. However, it is clear that we only need to compute the level set function near grain surfaces. It is possible to achieve this goal since we know where each interface is located, i.e., at $u = 0$. Therefore, we only compute the level set function in a narrow band around each surface. This approach is called the narrow band level set method. Although we have made several important modifications specifically for this problem, we have followed the spirit of this approach as outlined by Adalsteinsson and Sethian [22] and Peng et al. [23]. To further save memory we dynamically allocate memory for multiple level set functions. This helps because as the film grows some grains grow more than others and as a consequence need more memory. In addition, the narrow band has an active part and an inactive part. The active part is where the crystals are growing and the inactive part is where the crystals have grown into each other and no further growth occurs. The inactive parts are removed from memory and stored on disk. In this way, we are able to perform computations with over 200 level set functions on grids as large as $350 \times 350 \times 1200$ on a computer with 1 GB of RAM.

In the simulation presented here, we employ periodic boundary conditions on the edges of the computational cell in the direction parallel to the substrate plane in order to reduce the effects of a finite size computational domain. We have performed numerical convergence studies and determined that a computational mesh of size 250×250 produces solutions of sufficient accuracy. For our initial conditions, we placed 121 very small grains (islands) at random locations on the substrate with random orientations. This was done as follows: each seed was rotated using the three Euler angles, the first and last were taken uniformly in $[0, 2\pi]$ whereas the second was such that its cosine is uniform in $[-1, 1]$. In this way the distribution of orientations is isotropic. All the seeds were of the same size and their centers were all at the same height. The average height of the film, h, is expressed in terms of the average distance between the grains at the beginning of the simulation, d_0.

The results for average grain size, roughness of the surface and orientation distribution are averaged over a dozen runs.

4. Surface morphology and crystallographic texture

In this section and in the next two we report the results about macroscopic parameters concerning the polycrystal. Most of them, such as texture, cross-sections, and grain size, are computed after the crystal is grown, by cutting slides of the crystal at a given height h, and by measuring the desired parameters from the cross-section. Surface morphology and surface roughness (see Section 6), however, are computed during the run.

Figs. 2–6 show the surface morphology as a function of film thickness, h, during the growth of the film. Since the physics of the growth contains nothing to break the in-plane (plan view) symmetry, we characterize the crystallographic texture as a fiber texture. To this end, we focus specifically on the value of θ for each grain, weighting each grain according to the projection of the surface area on the x–y plane, and constructing the corresponding fiber texture distribution functions. These are shown beneath the corresponding surface morphology in Figs. 2–6.

Examination of the texture distribution functions shows that as the film thickens, the texture distribution sharpens into a pronounced fiber texture. The distribution becomes sharply peaked at an orientation, $\theta_{\max}$ that varies with α. To see this more clearly, we have plotted $\theta_{\max}$ as a function of α in Fig. 8. $\theta_{\max}$ decreases from 52° to 5° as α increases from 1 to 2.9. Fig. 8 also shows

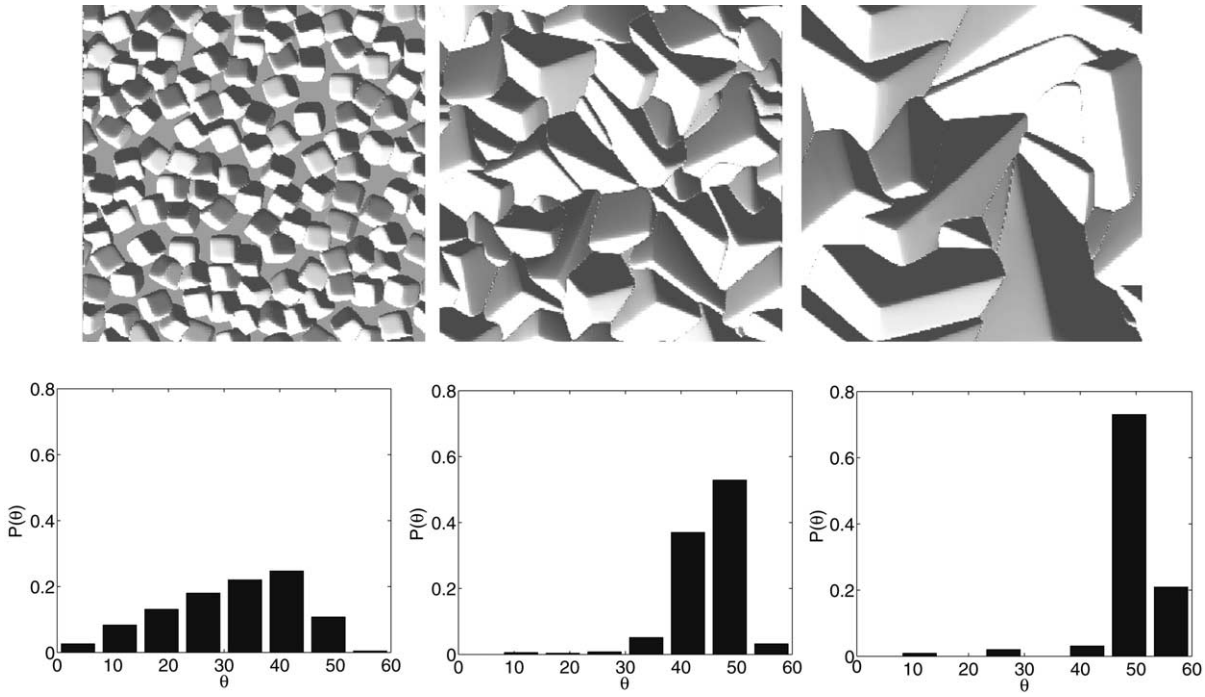

Fig. 2. Surface morphology (upper row) and orientation distribution function (lower row) evolution for $\alpha = 1$. From left to right, $h = 0.36d_0$, $h = 12.0d_0$, and $h = 36.2d_0$.

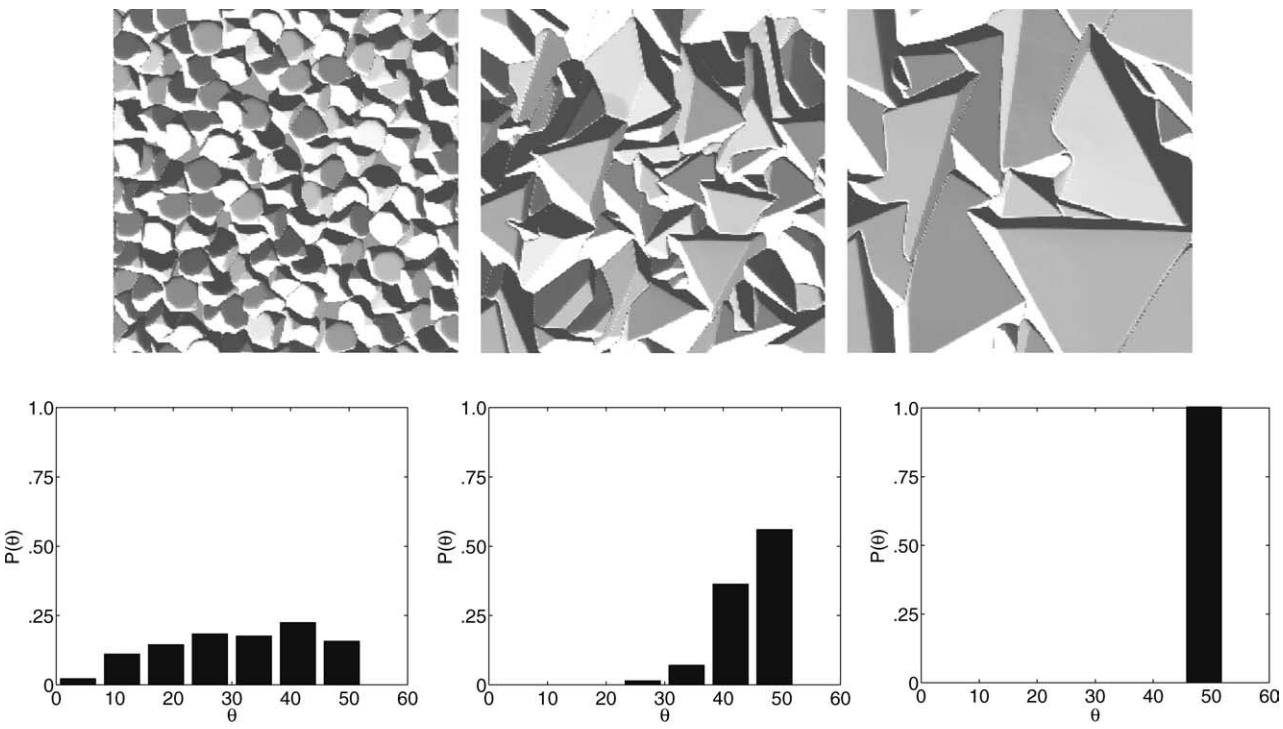

Fig. 3. Surface morphology (upper row) and orientation distribution function (lower row) evolution for $\alpha = 1.1$. From left to right, $h = 0.55d_0$, $h = 8.0d_0$, and $h = 27.0d_0$.

the theoretical prediction of $\theta_{\max}$ (i.e. Eq. (2)). The simulation data are in very good agreement with the theoretical predictions (within the statistical error in the simulations). This suggests that the orientation of the fiber texture $\theta_{\max}$ is accurately characterized by the assumption that $\theta_{\max}$ is simply the fastest growing direc-

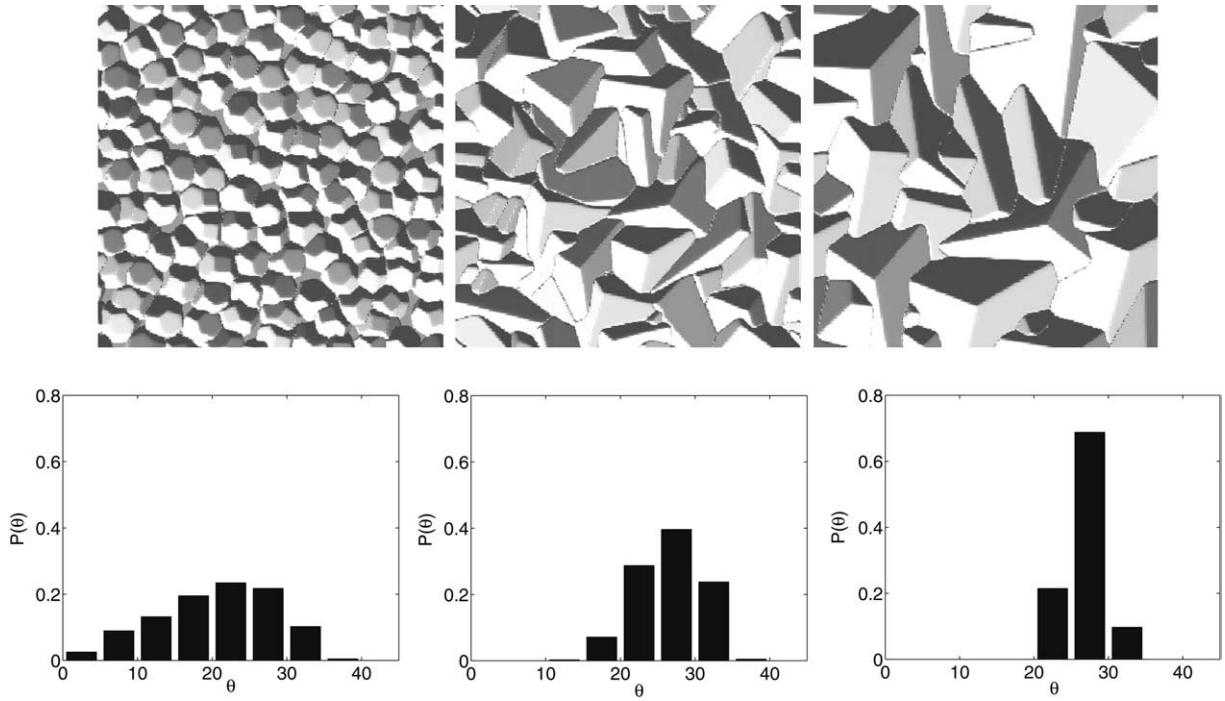

Fig. 4. Surface morphology (upper row) and orientation distribution function (lower row) evolution for $\alpha = 2$. From left to right, $h = 0.50d_0$, $h = 11.0d_0$, and $h = 40.0d_0$.

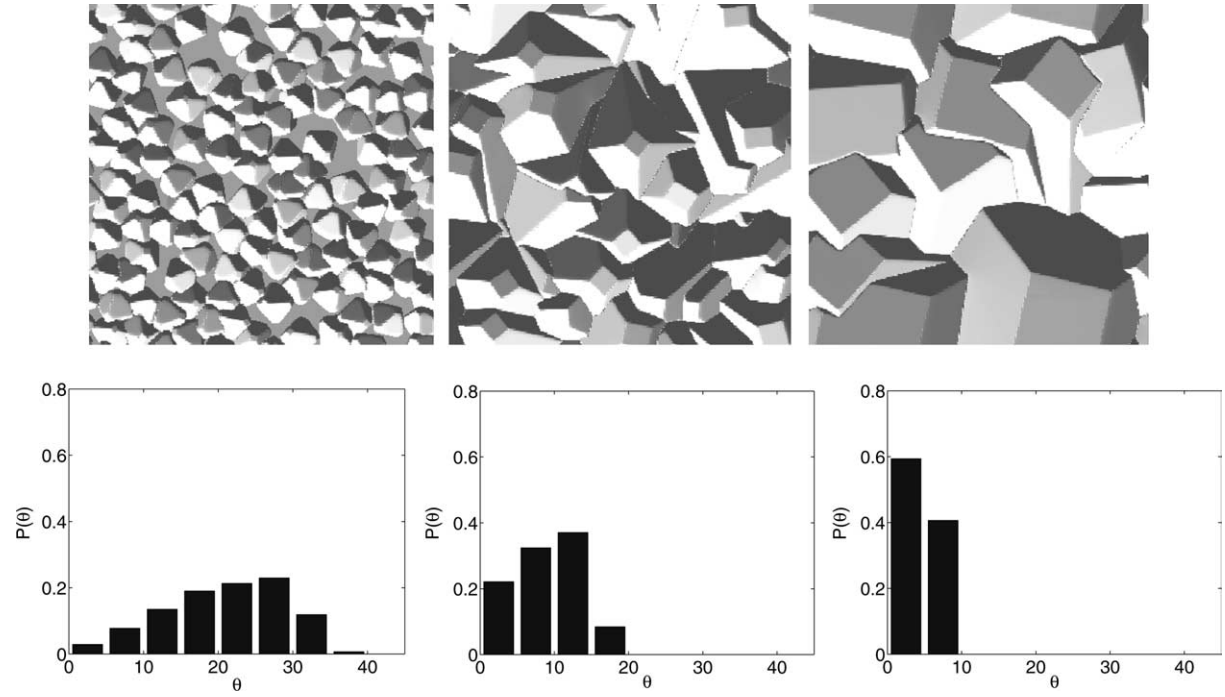

Fig. 5. Surface morphology (upper row) and orientation distribution function (lower row) evolution for $\alpha = 2.9$. From left to right, $h = 0.70d_0$, $h = 11.0d_0$, and $h = 43.0d_0$.

tion in the idiomorph (kinetic Wulff shape) and that direction is oriented normal to the substrate. In other words, $\theta_{\max}$ corresponds to the crystallographic direction specified in Eq. (4).

We now consider the observed polycrystalline surface morphology seen in Figs. 2–6 in more detail. Fig. 2 shows the case of $\alpha = 1$, where the kinetic Wulff shape (Fig. 1) is a cube. The fastest growing direction (longest

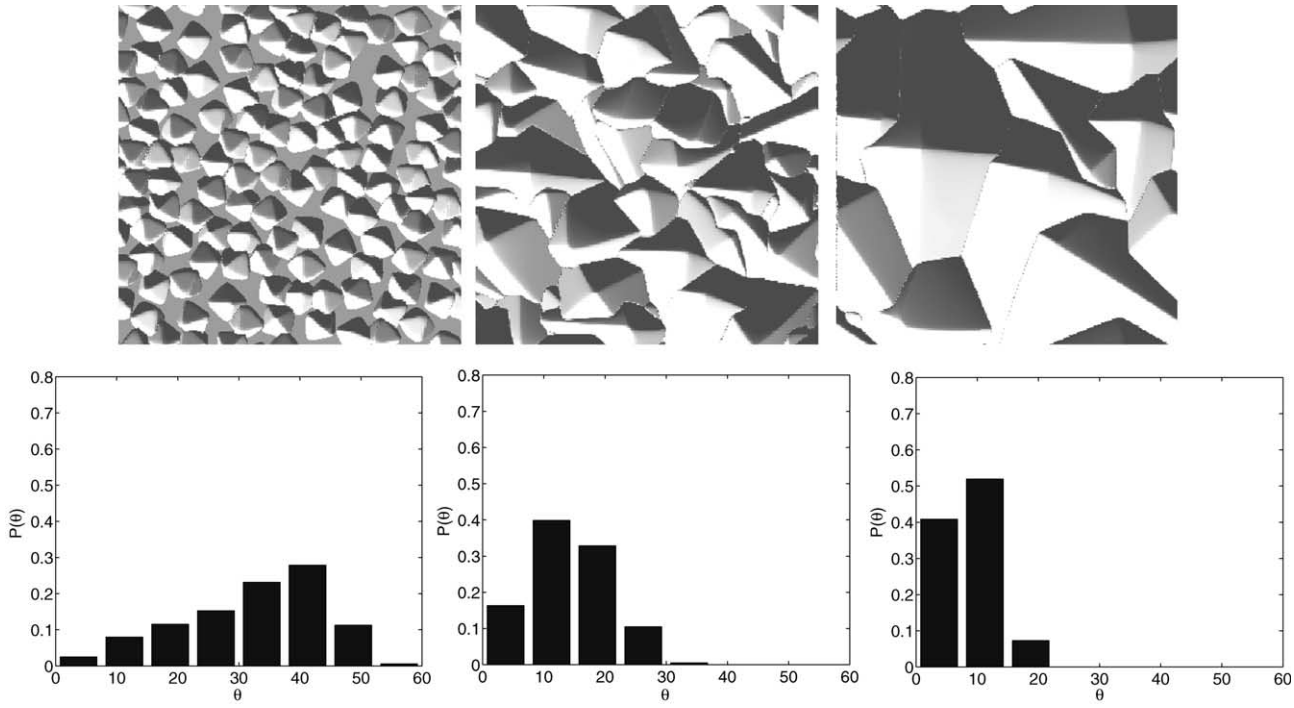

Fig. 6. Surface morphology (upper row) and orientation distribution function (lower row) evolution for $\alpha = 3$. From left to right, $h = 0.40d_0$, $h = 10.0d_0$, and $h = 37.0d_0$.

vector from the center of the kinetic Wulff shape) is $\langle 1\,1\,1\rangle$ in this case. Indeed, the surface morphology evolves such that the grains with $\langle 1\,1\,1\rangle$-directions are normal to the plane of the surface. $\theta_{\max}$ for this case ($\alpha = 1$) is 52°, while the analytical prediction based on the kinetic Wulff shape analysis (Eq. (2)) is $\tan^{-1}\sqrt{2} = 54.73°$. Further, the surface morphology appears as if it is composed of cubes viewed along the body diagonal - three flat surfaces meet at a point and each pair of planes meet at 90°. These planes are all $\{0\,0\,1\}$-planes, as predicted by the kinetic Wulff shape.

Fig. 3 shows the surface morphology for the $\alpha = 1.1$ case. The surface morphology changes dramatically with the change in α from 1.0 (Fig. 2) to 1.1. This may be surprising because the location of the peak in the orientation distribution only suffered a small shift upon this change in α. For $\alpha = 1.1$, the surface is largely composed of triangular facets that are nearly parallel with the mean surface and no corners point out of the surface, as they did for $\alpha = 1$. The triangular facets are of the $\{1\,1\,1\}$-type and the facets bounding the triangles are of the $\{0\,0\,1\}$-type. Such surface morphologies were previously observed in CVD diamond films; see for example Barrat and Bauer-Grosse [25] and May [26]. To understand this surface morphology, we return to the kinetic Wulff shapes of Fig. 1. For α infinitesimally larger than 1, the $\langle 1\,1\,1\rangle$ corners present in the $\alpha = 1$ cubic kinetic Wulff shapes are replaced with small triangular $\{1\,1\,1\}$ facets. These facets are nearly perpendicular to the fastest growing direction (slightly off of $\langle 1\,1\,1\rangle$: $\theta = \tan^{-1}\sqrt{2} = 54.73°$, $\phi = \pi/4$) and hence they are nearly parallel to the substrate. The $\{0\,0\,1\}$ facets bounding the triangles in the surface morphology can be traced to the $\{0\,0\,1\}$ surfaces of the kinetic Wulff shape that bounds the $\{1\,1\,1\}$ surface. Comparison of the orientation distribution plots in Figs. 2 and 3 demonstrates that the texture sharpens more quickly for $\alpha = 1.1$ than for $\alpha = 1.0$.

Fig. 4 shows the surface morphology and orientation distribution function for the $\alpha = 2$ case. The morphology is characterized by corners that poke out from the mean surface plane. Although it is not obvious from this figure, the surface is composed of both $\{1\,1\,1\}$ and $\{0\,0\,1\}$ facets- two $\{1\,1\,1\}$ and one $\{0\,0\,1\}$ facet meet at each corner. This morphology is consistent with the predictions drawn from the kinetic Wulff shape, as discussed above. The orientation distribution plots and Fig. 8 demonstrate that $\theta_{\max} \approx 27°$ from the simulations, which is in reasonable agreement with the prediction of $\theta_{\max} = 26.6°$ from Eq. (2). This corresponds to a $\langle 0\,1\,2\rangle$ fiber texture.

The results for $\alpha = 2.9$ are shown in Fig. 5. This surface shows pronounced square $\{0\,0\,1\}$ facets, as compared with the previous figure ($\alpha = 2$). This surface morphology is similar to that seen in the experiments of, for example, May [26], and von Kaenel et al. [27] on CVD diamond. The square facets are parallel to the substrate and are consistent with the kinetic Wulff shape (Fig. 1). In this case, the fastest growing direction (and hence the mean surface normal) is close to $\langle 0\,0\,1\rangle$

and, not surprisingly, the {0 0 1} surfaces are nearly perpendicular to the fastest growing directions. In general, as the fastest growing direction in the kinetic Wulff shape becomes closer to an existing facet normal, the shape of that facet in the kinetic Wulff shape becomes more prominent in the overall surface morphology.

Fig. 6 shows the surface morphology for the $\alpha = 3$ case. The surface morphologies for $\alpha = 2.9$ and 3.0 are quite different. Unlike in the $\alpha = 2.9$ case, this surface exhibits no square facets and no three-fold corners (i.e., points where three facets meet). The lack of square facets is attributable to the fact that the only facets seen are of the {1 1 1} type. The corners are all junctions of four {1 1 1} facets. This is consistent with the bipyramid kinetic Wulff shape for $\alpha = 3$ (see Fig. 1). As the film thickens, the orientation distribution sharpens and $\theta_{\max}$ decreases. By the end of the simulation, $\theta_{\max} \approx 8°$ which is close to the predicted value of $\theta_{\max} = 0$. However, $\theta_{\max}$ is still decreasing and we expect that $\theta_{\max} \to 0$ as $h \to \infty$.

Finally, Fig. 7 presents the surface morphology at fixed film thickness for $\alpha = 1.45$, $\alpha = 1.5$, and $\alpha = 1.55$. $\alpha = 1.5$ is a bifurcation point in the kinetic Wulff shape (see Fig. 1). As α increases from below 1.5 to above 1.5 the {1 1 1} facets change from equilateral triangles to 6-sided polygons and the {0 0 1} facets change from octagonal to square. This transition in the kinetic Wulff shape is manifested in the film surface morphology, although it is not as striking as the changes that occur when α increases from 1 to 1.1 or 2.9 to 3. For $\alpha = 1.45$ the surface of the film has "roof-shaped structures" [3] (two sides are {0 0 1} facets and the other is a {1 1 1} facet), whereas when $\alpha = 1.55$ the film is composed of 3-sided peak-like structures (one side is a {0 0 1} facet and the other two are {1 1 1} facets). It is evident from Fig. 7 that the distribution of θ changes little as α is varied from 1.45 to 1.55. The peak occurs for $\theta \approx 45°$; this corresponds to a $\langle 0\,1\,1 \rangle$ fiber texture. The present $\alpha = 1.45$ surface morphology is very similar to that observed in experiment by Wild et al. [3] and the surface morphology computed for $\alpha = 1.5$ was seen in

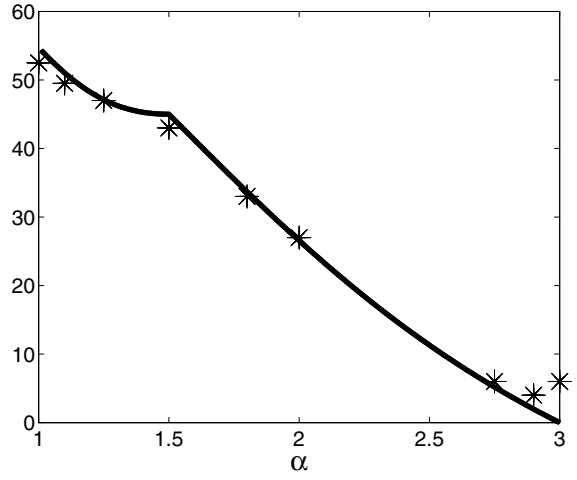

Fig. 8. $\theta_{\max}$ as a function of α. The data points represent the average value of θ computed from our simulations and the curve is the theoretical prediction of [7].

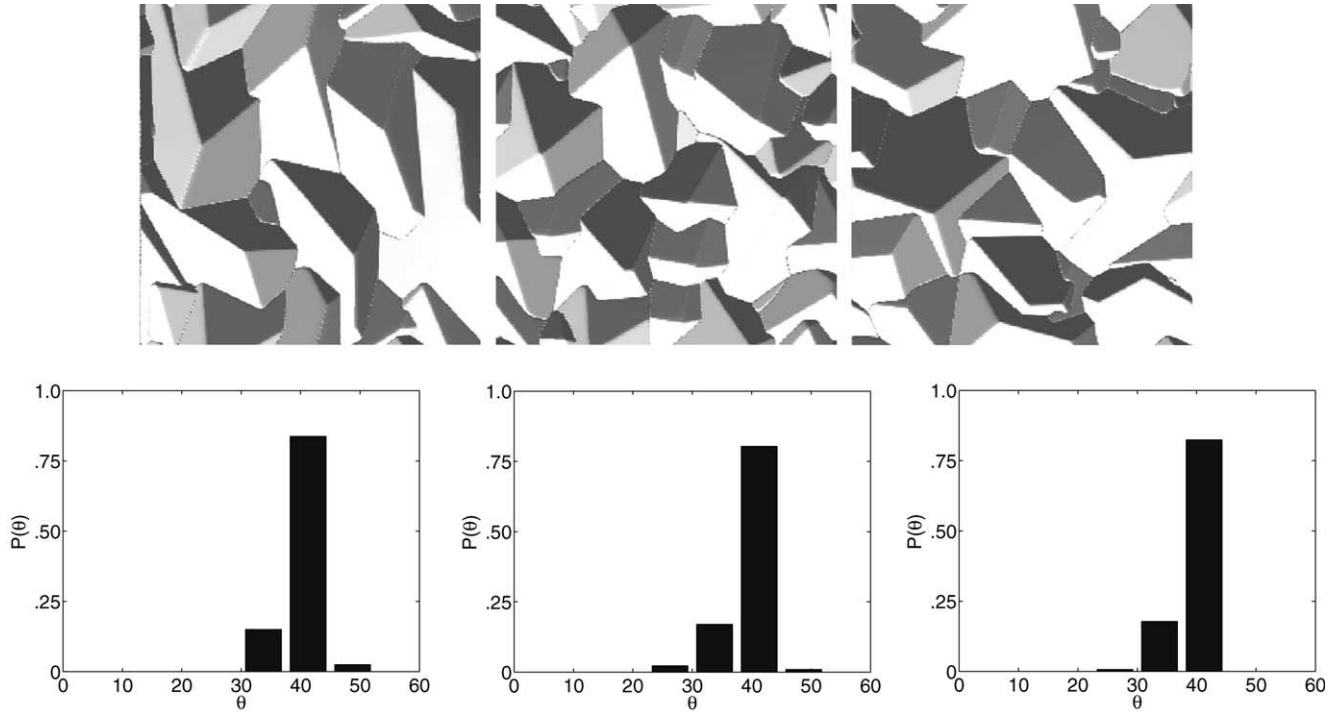

Fig. 7. Surface morphology (upper row) and orientation distribution function (lower row) corresponding to $\alpha = 1.45$, $\alpha = 1.5$, and $\alpha = 1.55$ (from left to right) at $h = 20d_0$.

the experimental work of Barrat and Bauer-Grosse [25] in diamond.

5. Cross-sections

The level set film growth algorithm also gives us the ability to view cross-sections of the grown film and thereby examine the polycrystalline microstructure through the film thickness. Fig. 9 shows three different cross-sections of films grown with different values of α. In all cases, the mean grain size increases with height, the grains are very elongated in the direction of growth (i.e., columnar growth) and new grains appear and disappear in the cross-section (above the substrate/film interface). These are all commonly observed features of cross-sections in a very wide variety of films, including diamond. The disappearance of grains is, in some cases, the result of growth competition, where a growing grain is overgrown by its neighbors. In other cases, the grain may appear to disappear simply because the grain boundary is extending into a direction with a component normal to the plane of the cross-section. The same visual effect explains the apparent "nucleation" of new grains above the substrate/film interface (i.e. a boundary of a grain that is behind the cross-section extends into a direction with a component normal to the plane of the cross-section of observation).

It is interesting to compare these cross-sections with the results of the two-dimensional simulations of Paritosh et al. [7]. Overall, the main features of the present cross-sections of the three-dimensional films are quite similar to those from the two-dimensional simulations. The most striking difference between the three-dimensional and the two-dimensional cross-sections is the apparent grain "nucleation" events in the three-dimensional case which are completely absent in the two-dimensional case. This difference is simply that the grain boundaries cannot extend in the direction perpendicular to the plane of the cross-section in two-dimensions, while this effect can (and does) occur in three dimensions.

6. Grain size and roughness

The evolution of the average grain size (as measured in plan view) with film thickness, h, is shown in a double logarithmic plot in Fig. 10. The precise definition of grain size, and surface roughness are re-

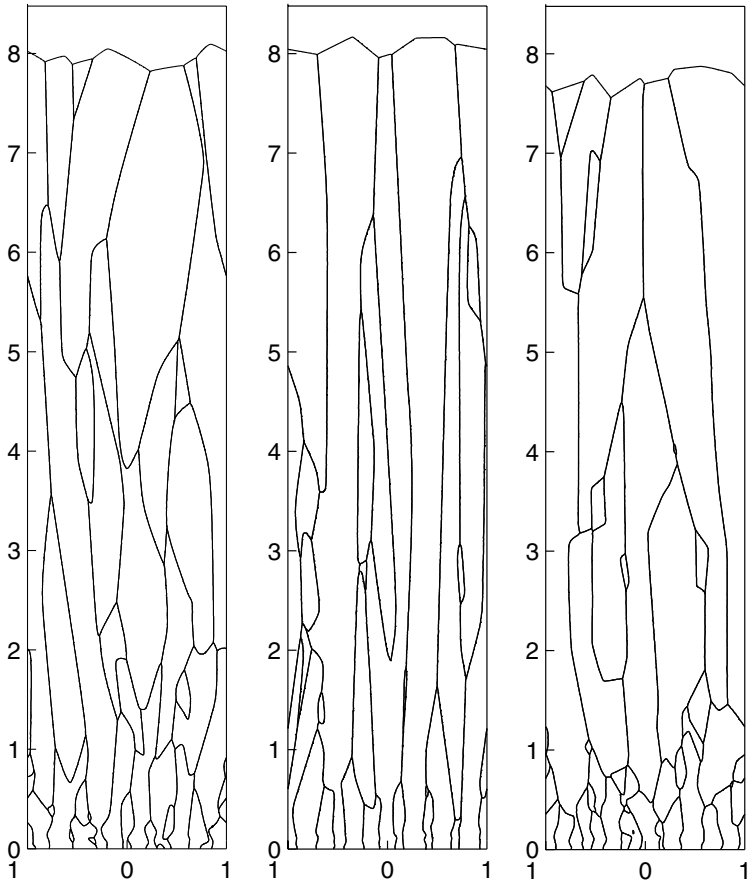

Fig. 9. Cross-sectional view of the film, showing the grain boundaries in the polycrystalline structure and the growth front. This figure shows that the grain size increases with thickness and that the microstructure is columnar. The three micrographs corresponds to $\alpha = 1$, 2 and 2.9, from left to right.

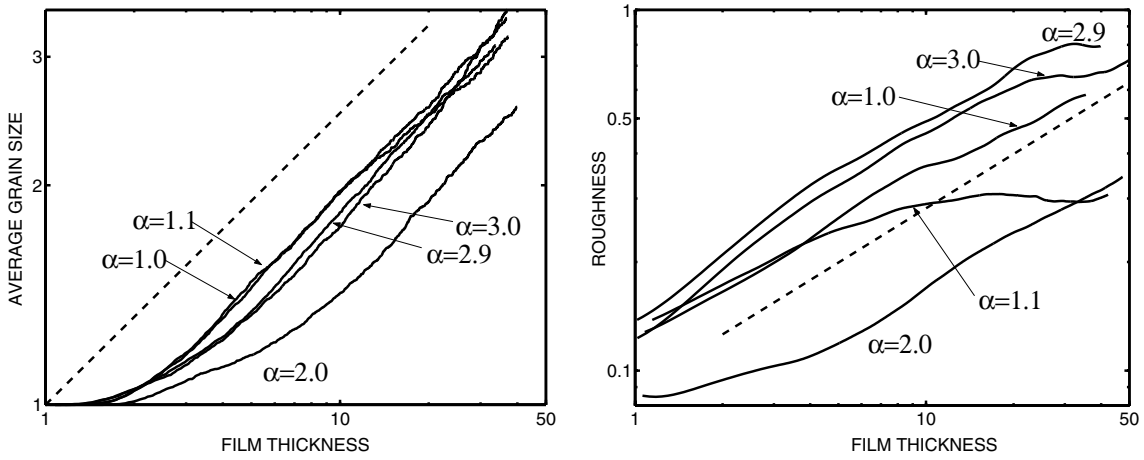

Fig. 10. The figure on the left shows a plot of the scaled average grain size versus the scaled mean film thickness in double logarithmic coordinates. The figure on the right shows a log–log plot of the roughness vs. average film height. In both plots, we include a straight line of slope 2/5 to aid comparisons with theory.

ported in Appendix A. Following an initial transient associated with the growth of the seeds to impingement, the average grain size, d, increases with h as $d \propto h^{\beta}$, where the best fit value of the large thickness data is $\beta = 0.42 \pm 0.03$. The two-dimensional simulation data [7] suggest that $\beta \approx 0.5$. Theoretical predictions by Kolmogorov [8] and Thijssen et al. [9] indicate that $\beta = 0.5$ in two dimensions and Thijssen [10] predicted $d \sim h^{2/5}$ in three dimensions. The present results are consistent with Thijssen's three-dimensional predictions to within the fitting error.

Fig. 10 also shows how the root mean square surface roughness, w, evolves with film thickness for several values of α. We first focus on the $\alpha = 1$ and 3 cases. The roughness, w, grows with film thickness as $w \propto h^{\beta}$, where $\beta = \frac{2}{5}$ (cf. the curves with the straight line in the figure). This is to be expected since the grain size grows as h^{β}. Similar behavior was observed by Paritosh et al. [7] in two dimensions. The $\alpha = 2$ data in Fig. 10 yield the same value of β as do the $\alpha = 1$ and 3 cases. However, this curve is shifted to greater thicknesses. This too is expected since the grain size evolves slowly for $\alpha = 2$. Only the $\alpha = 1.1$ data show significant differences as compared to those for the other α's. The initial evolution of the roughness in this case is the same as for the other values of α, but the slope (exponent) decreases to near zero at larger film thickness. The origin of this decrease in slope is not fully understood, but similar behavior was observed in the two-dimensional simulation of Paritosh et al. [7] for α near the end points of the range (1–2 in two dimensions). We note that for $\alpha = 1.1$ the fastest growing direction is approximately normal to the {1 1 1} facet, which should produce a low roughness surface (as observed – see Fig. 3). On this basis, we should expect similar behavior for $\alpha = 2.9$, where the fastest growing direction is approximately normal to the

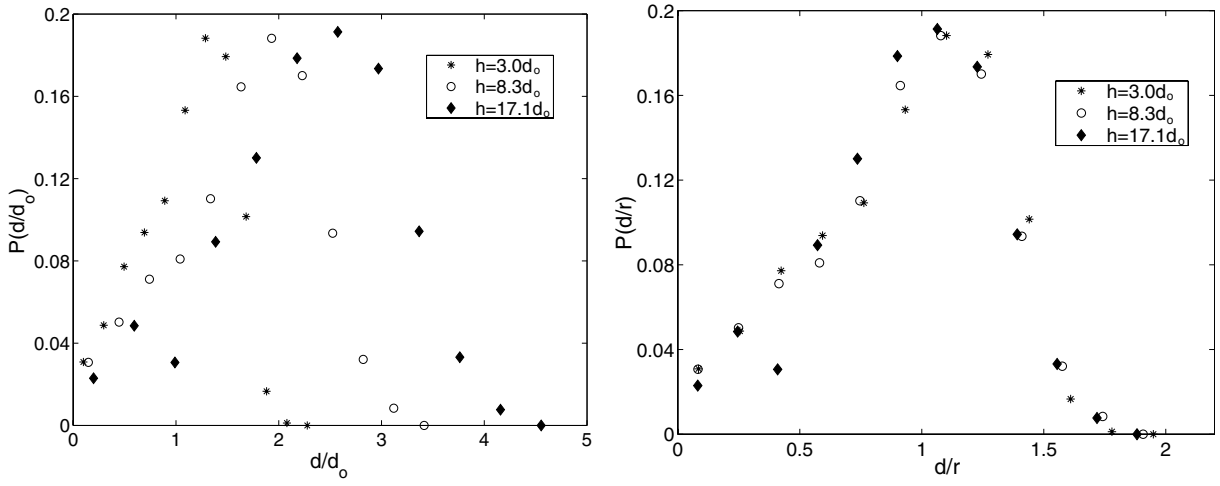

Fig. 11. The figure on the left shows the grain size distribution and the figure on the right shows the grain size distribution scaled by the evolving mean film height.

{001} facet. However, this is not observed in Fig. 10. Nevertheless, it is possible that such an effect would be seen for thicker films.

Fig. 11 shows the grain size distribution at several different film heights for the $\alpha = 2.9$ case. This distribution clearly evolves during film growth. However, if we scale the grain size by the mean film thickness, the distributions collapse onto one another. This indicates that the grain size distribution is self-similar when scaled by the average grain size. Similar behavior was found for the other values of α. Similar results were reported by Paritosh et al. [7] in two dimensions. This is the first demonstration that the scaling law observed in two dimensions is also valid in three dimensions.

7. Discussion and conclusions

Although the present report focused mainly on the application of the level-set method for faceted, polycrystalline film growth to the growth of diamond, both the method and the conclusions are much more general. Application to diamond was motivated by the existence of an extensive experimental literature of growth morphologies, texture and grain size versus growth conditions (α). The only choice made in these simulations specifically for diamond was the limitation of consideration to {111} and {001} facets. The results should be equally applicable to other cubic materials exhibiting these types of facets. Extensions of the model to include other facets, e.g., {011}, is straightforward, but requires the introduction of another variable for each new type of facet corresponding to its relative velocity, $\alpha_1 \sim \frac{V_{001}}{V_{111}}$, $\alpha_2 \sim \frac{V_{011}}{V_{111}}$,... The method is also readily applicable to cases where grain nucleation is non-random, the surface contains overhangs (forbidden in many other models, such as solid-on-solid), and other crystal structures. For example, Fig. 12 shows a case of the growth of a polycrystalline film of a tetragonal crystal structure where only {001} facets are possible and the ratio of the growth rate of the {001} facet is much faster than the {100} facets (i.e., $V_{001} \gg V_{100} = V_{010}$). This results in a complex microstructure of needle-like grains – complete with overhangs.

The main results of the present simulation study may be summarized as follows. Faceted, polycrystalline film growth produces a microstructure of columnar grains and a surface morphology that compare favorably to a wide range of experimental observations of diamond film growth. The film develops a fiber texture that sharpens as it grows. The axis of this fiber texture is oriented perpendicular to the substrate and is determined by the relative growth rates of the facets. These texture observations are also consistent with experiment. The mean grain size, d, scales with film thickness, h as $d \sim h^{2/5}$. In most cases, the roughness scales with thickness with the same exponent.

Many of the main features observed in the surface morphology and crystallographic texture can be understood in terms of the kinetic Wulff shape or idiomorph, as suggested by others [3,4]. This approach was extended by Paritosh et al. [7] and here. We note that the grain size and roughness exponent is different in two and three dimensions, i.e., 1/2 and 2/5, respectively. This is consistent with the predictions of Thijssen [10]. These results, together with the differences between the kinetic Wulff shape in two and three dimensions demonstrate the need to perform such simulations of film growth (and microstructure/morphology evolution) in the same number of dimensions as the real physical problem (i.e., usually three). While previous methods have been proposed to simulate polycrystalline, faceted film growth in three dimensions, the present simulations is the only one, to our knowledge, that is fully consistent with the underlying van der Drift model. Of these major results, we expect the existence of a faceted, fiber textured, columnar film structure and the grain size and roughness scaling relations to be a general feature of polycrystalline, faceted film growth, independent of the detailed assumptions of which facets appear, the crystal structure, and the relative facet growth rates.

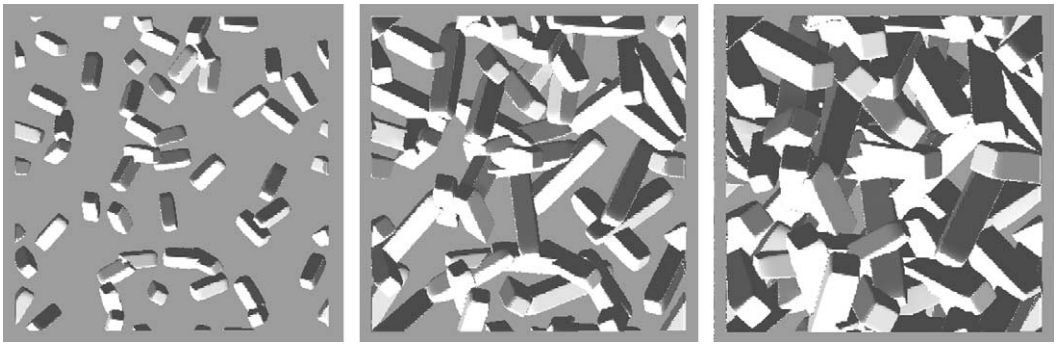

Fig. 12. Evolution of needle-like crystals.

Acknowledgements

P.S. gratefully acknowledges the support of the National Science Foundation though grants DMS-9625190 and DMS-0207402. D.J.S. gratefully acknowledges the support of the US Department of Energy through Grant DE-FG02-99ER45797. The authors acknowledge early support from DARPA through the VIP program. We also thank Silvère Barrat for kindly sending us a reprint of [25].

Appendix A. Definition of statistical observables

A.1. Grain size

The total height of the crystal is a function of time, and of two spatial coordinates. Let us express this in the form $h_s = h_s(t, x, y)$.

We measure the grain size by taking a cross-section of the crystal at a given height h. We shall make sure that the cross-section will not contain empty regions. This is guaranteed if $h < h_s(t_{max})$, where t_{max} is the final time of computation.

The cross-section is therefore formed by a tessellation of regions, corresponding to grains. Let us say that a given cross-section is formed by N_g two-dimensional grains. Then we define

$$d_i = \sqrt{A_i}, \quad i = 1, \ldots, N_g,$$

where A_i is the area of the ith grain of the cross-section. For a given h, the grain size distribution is obtained by plotting the histogram of the quantities d_i defined above.

The *average grain size* is defined as the square root of the average area of the grain. For one realization, at a given height h, it is

$$d = \sqrt{\langle A \rangle} = \sqrt{\frac{1}{N_g}\sum_{i=1}^{N_g} A_i} = \sqrt{\frac{A}{N_g}},$$

where A is the area of the computational domain. In all our calculation it was $A = 4$. For N realization of the process, then we define

$$d = \sqrt{\frac{NA}{\sum_{j=1}^{N} N_g^{(j)}}},$$

where $N_g^{(j)}$ is the number of seeds at the jth realization of the process (for a given height h).

All information about the grain size distribution can be obtained by a post-processing, at the end of the runs, from the information about the polycrystal stored in files. We assume that at the height we measure the grain size distribution the whole computational domain is occupied by grains, which is true if the cross-section does not intersects the surface of the polycrystal.

A.2. Surface roughness

For a given time, the average height, $\bar{h}(t)$, is given by

$$\bar{h}(t) = \frac{\int_\Omega h_s(t,x,y)\, dx\, dy}{A},$$

where Ω is the computational domain (with periodic boundary conditions), $A = |\Omega|$. The roughness of the surface is defined as the root mean square of the deviation of the height of the crystal surface from its average:

$$\text{roughness} = \omega(t) = \sqrt{\frac{\int_\Omega (h_s(t,x,y) - \bar{h}(t))^2}{A}}.$$

Of course the integrals are approximated on the computational grid by the midpoint rule. The plot of roughness versus thickness are obtained by plotting ω versus $\bar{h}$ (on a logarithmic scale).

At variance with the information about grain size, surface roughness has to be computed during the run, since it depends on the actual surface of the polycrystal, and not on its cross-sections.

References

[1] van der Drift A. Evolutionary selection, a principle governing growth orientation in vapor-deposited layers. Philips Res Rep 1967;22:267.
[2] Thompson CV. Structure evolution during processing of polycrystalline films. Annu Rev Mater Sci 2000;30:159–90.
[3] Wild C, Herres N, Koidl P. Texture formation in polycrystalline diamond films. J Appl Phys 1990;68(3):973.
[4] Wild C, Koidl P, Müller-Sebert W, Walcher H, Kohl R, Herres N, et al. Chemical-vapor-deposition and characterization of smooth (1 0 0)-faceted diamond films. Diam Relat Mater 1993;2:158.
[5] Wild C, Koidl P, Herres N, Müller-Sebert W, Koidl P. Oriented CVD diamond films – twin formation, structure and morphology. Diam Relat Mater 1994;3:373.
[6] Dammers AJ, Radelaar S. 2-Dimensional computer modeling of polycrystalline growth. Textures Microstruct 1991;14:757–62.
[7] Paritosh, Srolovitz DJ, Battaile CC, Li X, Butler JE. Simulation of faceted film growth in two-dimension: microstructure morphology, and texture. Acta Mater 1999;47:2269.
[8] Kolmogorov AN. To the "geometric selection" of crystals. Dok Acad Nauk USSR 1940;65:681–4.
[9] Thijssen JM, Knops HJF, Dammers A. Dynamic scaling in polycrystalline growth. Phys Rev B 1992;45:8650–6.
[10] Thijssen JM. Simulations of polycrystalline growth in 2 + 1 dimensions. Phys Rev B 1995;25:1985–8.
[11] Barrat S, Pigeat P, Bauer-Grosse E. Three-dimensional simulation of CVD diamond film growth. Diam Relat Mater 1996;5:276–80.
[12] Russo G, Smereka P. A level set method for the evolution of faceted interfaces. SIAM J Sci Comput 2000;6:2073–95.
[13] Osher S, Sethian J. Fronts propagating with curvature-dependent speed: algorithms based on Hamilton–Jacobi formulation. J Comput Phys 1988;79:12–49.

[14] Sethian JA. Level set methods: evolving interfaces in geometry, fluid mechanics, computer vision, and materials sciences. Cambridge: Cambridge University Press; 1996.
[15] Osher S, Fedkiw R. Level set methods and dynamic implicit surfaces. New York: Springer; 2000.
[16] Smereka P, Sethian JA. Level set methods for fluid interfaces. Annu Rev Fluid Mech 2003;35:341–72.
[17] Taylor JE, Cahn J, Handwerker CA. Geometrical models of crystal growth. Acta Metall Mater 1992;40:1443–74.
[18] Osher S, Merriman B. The wulff shape as the asymptotic limit of a growing crystalline interface. Asian J Math 1997;1:560–71.
[19] Peng D, Osher SJ, Merriman B, Zhao HK. The geometry of Wulff crystal shapes and its relations with Riemann Problems. In: Chen G-Q, Benedetto ED, editors. Contemporary Mathematics vol. 238. Providence: AMS; 1999, p. 251–303.
[20] Wulff G. Frage der geshwindigkeit des wachstums und der anflosung der kristallflachen. Z Krystall Min 1901;34: 449–530.
[21] Frank FC. On the kinematic theory of crystal growth and dissolution processes. Growth and perfection of crystals. In: Doremus D, Roberts BW, Turnbull D, editors. Growth and perfection of crystals. New York: John Wiley; 1958.
[22] Adalsteinsson D, Sethian JA. A fast level set method for propagating interfaces. J Comput Phys 1995;118:269–77.
[23] Peng DP, Merriman B, Osher S, Zhao HK, Kang MJ. A PDE-based fast local level set method. J Comput Phys 1999;155: 410–38.
[24] Barrat S, Dieguez I, Michel H, Bauer-Grosse E. Morphometric analysis of diamond crystals elaborated by microwave plasma assisted chemical vapour deposition application to textured films. Diam Relat Mater 1994;3:520–4.
[25] Barrat S, Bauer-Grosse E. Prediction of the feasibility or oriented diamond films by microwave plasma-assisted CVD. Diam Relat Mater 1995;4:419–24.
[26] May PW. Diamond thin films: a 21st-century material. Phil Trans Roy Soc Lond A 2000;358:473–95.
[27] von Kaenel Y, Stiegler J, Blank E, Chauvet O, Hellwig Ch, Plamann K. Microstructure evolution and defect incorporation in highly oriented and textured CVD diamond films. Phys Status Solidi (a) 1996;154:219–38.